



Limitations of Surface Liquefaction Manifestation Severity Index Models Used in Conjunction with Simplified Stress-Based Triggering Models

Sneha Upadhyaya, S.M.ASCE¹; Russell A. Green, F.ASCE²; Brett W. Maurer, M.ASCE³; Adrian Rodriguez-Marek, M.ASCE⁴; and Sjoerd van Ballegooy⁵

Abstract: The severity of surface manifestation of liquefaction is commonly used as a proxy for liquefaction damage potential. As a result, manifestation severity index (MSI) models are more commonly being used in conjunction with simplified stress-based triggering models to predict liquefaction damage potential. This paper assesses the limitations of three existing MSI models and a fourth MSI model that is developed herein. The different models have differing attributes that account for factors influencing the severity of surficial liquefaction manifestations, with the newly proposed model accounting more factors than the others. The efficacies of these MSI models are evaluated using well-documented liquefaction case histories from Canterbury, New Zealand, with the deposits primarily comprising clean to nonplastic silty sands. It is found that the MSI models that explicitly account for the contractive/dilative tendencies of soil did not perform as well as the models that do not account for this tendency, opposite of what would be expected based on the mechanics of liquefaction manifestation. The likely reason for this is the double-counting of the dilative tendencies of medium-dense to dense soils by these MSI models because the liquefaction triggering model, to some extent, inherently accounts for such effects. This implies that development of mechanistically more rigorous MSI models that are used in conjunction with simplified triggering models will not necessarily result in improved liquefaction damage potential predictions and may result in less accurate predictions. This provides the impetus for the development of a new framework that clearly and distinctly separates triggering and manifestation. DOI: 10.1061/(ASCE)GT.1943-5606.0002725. © 2021 American Society of Civil Engineers.

Introduction

The objective of this study is to assess the limits of predicting the occurrence and severity of surficial liquefaction manifestation via manifestation severity index (MSI) models that are used in conjunction with simplified stress-based triggering models. The severity of surficial liquefaction manifestation is often used as a proxy for liquefaction-induced damage potential for near-surface infrastructure. As such, accurate prediction of the severity of surficial liquefaction manifestation is critical for reliably assessing the risk due to liquefaction. This requires a proper understanding of the mechanics of the manifestation of surficial liquefaction features and the controlling factors.

Past studies have shown that surficial liquefaction manifestation is governed by several factors, including (1) properties of the

Note. This manuscript was submitted on April 13, 2021; approved on September 28, 2021; published online on December 22, 2021. Discussion period open until May 22, 2022; separate discussions must be submitted for individual papers. This paper is part of the *Journal of Geotechnical and Geoenvironmental Engineering*, © ASCE, ISSN 1090-0241.

liquefied strata such as the depth, thickness, density, fines content, and posttriggering strain potential; (2) properties of the nonlique-fied soil strata (i.e., those of the crust/capping layer and/or layers interbedded within the liquefiable soil) such as fines content, plasticity, permeability, and thickness; and (3) the stratification/ sequencing of the liquefied and nonliquefied strata and the cross-interaction between these layers within a soil profile (e.g., Iwasaki et al. 1978; Ishihara and Ogawa 1978; Ishihara 1985; van Ballegooy et al. 2012, 2014b; Maurer et al. 2015a, d; Upadhyaya et al. 2018; Beyzaei et al. 2018; Cubrinovski et al. 2019; among others).

Different models have been proposed in the literature to predict the occurrence/severity of surficial liquefaction manifestation, usually in the form of a numerical index (i.e., MSI models). These models use the results from simplified stress-based liquefaction triggering models and tie the cumulative response of the soil profile to the occurrence/severity of surficial liquefaction manifestation. However, the different models have differing attributes that account for factors influencing the severity of surficial liquefaction manifestations. One of the earliest MSI models is the liquefaction potential index (LPI), proposed by Iwasaki et al. (1978), which considers the influence of depth, thickness, and relative density (D_r) of the liquefiable layers through the factor of safety (FS) (e.g., for a given level of seismic demand, FS increases as D_r increases) to predict the severity of manifestation.

Although LPI has been widely used to characterize the damage potential of liquefaction throughout the world (e.g., Sonmez 2003; Papathanassiou et al. 2005; Baise et al. 2006; Papathanassiou 2008; Cramer et al. 2008; Hayati and Andrus 2008; Holzer et al. 2006, 2009; Holzer 2008; Yalcin et al. 2008; Chung and Rogers 2011; Dixit et al. 2012; Sana and Nath 2016; among others), it was found to perform inconsistently during the 2010–2011

¹Graduate Student, Dept. of Civil and Environmental Engineering, Virginia Tech, Blacksburg, VA 24061. Email: usneha@vt.edu

²Professor, Dept. of Civil and Environmental Engineering, Virginia Tech, Blacksburg, VA 24061 (corresponding author). ORCID: https://orcid.org/0000-0002-5648-2331. Email: rugreen@vt.edu

³Assistant Professor, Dept. of Civil and Environmental Engineering, Univ. of Washington, Seattle, WA 98195. Email: bwmaurer@uw.edu

⁴Professor, Dept. of Civil and Environmental Engineering, Virginia Tech, Blacksburg, VA 24061. ORCID: https://orcid.org/0000-0002-8384-4721. Email: adrianrm@vt.edu

⁵Technical Director, Geotechnical, Tonkin + Taylor Ltd., 105 Carlton Gore Rd., Newmarket, Auckland 1023, New Zealand. Email: SVanBallegooy@tonkintaylor.co.nz

Canterbury earthquakes in New Zealand (e.g., Maurer et al. 2014, 2015a, b). This inconsistency can be attributed to limitations in the LPI formulation to appropriately account for some of the factors influencing surficial manifestation of liquefaction.

Specifically, the LPI formulation may not adequately account for the contractive/dilative tendencies of the soil on the potential consequences of liquefaction. For example, a dense and a loose sand stratum both having FS=0.8 could result in the same LPI value, but the associated consequences will likely be very different. Moreover, the LPI formulation assumes that surface manifestations will not occur unless FS<1. However, surficial manifestations related to liquefaction may occur due to elevated excess pore pressures during shaking even when $FS \ge 1$, particularly in loose deposits.

Additionally, the LPI formulation does not account for the limiting thickness of the nonliquefied crust and/or the effects of nonliquefiable, high-fines-content (FC), high-plasticity soils on the severity of surficial liquefaction manifestations. Although the influence of these effects could be accounted for by using different LPI manifestation severity thresholds [i.e., LPI values distinguishing between different manifestation severity classes (e.g., Maurer et al. 2015d; Upadhyaya 2019)], it is preferred to have a model that can explicitly account for these conditions in a less ad hoc manner.

In efforts to address some of the shortcomings in the LPI formulation, alternative MSI models have been proposed, such as the Ishihara-inspired LPI (LPI $_{ish}$) by Maurer et al. (2015a) and lique-faction severity number (LSN) by van Ballegooy et al. (2012, 2014b). A major improvement of LPI $_{ish}$ over LPI is that it explicitly accounts for the phenomenon of limiting crust thickness, where a nonliquefied capping stratum having an equal or greater thickness than the limiting crust thickness inhibits any surficial liquefaction manifestations regardless of the liquefaction response of the underlying strata. This attribute of the LPI $_{ish}$ model is derived from Ishihara's (1985) empirical relationship that relates the thicknesses of the nonliquefied crust (H_1) and liquefied stratum (H_2) to the occurrence of surficial liquefaction manifestations.

However, as with LPI, LPI $_{ish}$ does not explicitly account for the contractive/dilative tendencies of the soil on the severity of manifestations. The LSN formulation conceptually overcomes this limitation of LPI, as well as LPI $_{ish}$, in that it explicitly accounts for the additional influence of contractive/dilative tendencies of the soil via the Ishihara and Yoshimine (1992) relationship among FS, D_r , and the postliquefaction volumetric strain potential (ε_v). However, LSN does not account for the phenomenon of limiting crust thickness, which LPI $_{ish}$ does.

Based on the identified limitations of previously proposed MSI models, herein, a MSI model that accounts for the limiting-crust-thickness phenomenon and the effects of contractive/dilative tendencies of the soil on the severity of surficial liquefaction manifestations is proposed. The new model, termed LSN $_{ish}$, is derived by combining the positive attributes of LPI $_{ish}$ and LSN in a single formulation that mechanistically accounts for the limiting-crust-thickness phenomenon based on Ishihara's $H_1 - H_2$ boundary curves and the contractive/dilative tendencies of the soil on the severity of surficial liquefaction manifestation via the Ishihara and Yoshimine (1992) $FS-D_r$ - ε_v relationship. Similar to the derivation of LPI $_{ish}$ by Maurer et al. (2015a), the new index is derived as a conceptual and mathematical merger of the Ishihara (1985) H_1 - H_2 relationships and the LSN formulation.

In the following, overviews of LPI, LPI_{ish}, and LSN models are presented first, which are then followed by the derivation of the new MSI model, LSN_{ish}. Next, all four MSI models are evaluated using a large data set of liquefaction case histories from the 2010–2011

Canterbury earthquake sequence and the 2016 Valentine's Day earthquake that impacted Christchurch, New Zealand, and the MSI models' predictive efficiencies are assessed.

Overview of Existing Manifestation Severity Index Models

Liquefaction Potential Index

LPI is defined as follows (Iwasaki et al. 1978):

$$LPI = \int_0^{z_{\text{max}}} F_{LPI}(FS) \cdot w_{LPI}(z) dz \tag{1}$$

where FS = factor of safety against liquefaction triggering, computed using a liquefaction triggering model; z = depth below the ground surface (m); $z_{\rm max}$ = maximum depth considered, generally 20 m; and $F_{\rm LPI}(FS)$ and $w_{\rm LPI}(z)$ = functions that account for the weighted contributions of FS and z on surface manifestation. Specifically, $F_{\rm LPI}(FS) = 1 - FS$ for $FS \le 1$ and $F_{\rm LPI}(FS) = 0$ otherwise; and $w_{\rm LPI}(z) = 10$ –0.5z. Thus, LPI assumes that the severity of surface manifestation depends on the cumulative thickness of liquefied soil layers, the proximity of those layers to the ground surface, and the amount by which FS in each layer is less than 1.0. Given this definition, LPI can range from 0 to 100.

Ishihara-Inspired Liquefaction Potential Index

Using the data from the $1983\,\mathrm{M_w}$ 7.7 Nihonkai-Chubu and $1976\,\mathrm{M_w}$ 7.8 Tangshan earthquakes, Ishihara (1985) proposed a generalized relationship relating the thicknesses of the nonliquefiable crust (H_1) and underlying liquefied strata (H_2) to the occurrence of liquefaction-induced damage at the ground surface. This relationship was developed in the form of boundary curves, which separate cases with and without surficial liquefaction manifestation as a function of peak ground acceleration ($a_{\rm max}$), as shown in Fig. 1(a). The solid-line portion of the curves shown in Fig. 1(a) were based on data from these events, and the dashed-line portions of the curves were based on interpolation, extrapolation, and independ.

The H_1 – H_2 boundary curves indicate that for a given $a_{\rm max}$, there exists a limiting H_1 , thicker than which surficial liquefaction manifestations will not occur regardless of the value of H_2 (i.e., the limiting-crust-thickness phenomenon mentioned in the "Introduction"). Although Ishihara's H_1 – H_2 curves have been shown to perform well in some studies (e.g., Youd and Garris 1995), other studies have shown that the curves are not easily implementable for more complex soil profiles that have multiple interbedded nonliquefied/nonliquefiable soil strata, such as those in Christchurch, New Zealand (e.g., van Ballegooy et al. 2014b, 2015). Other issues with the Ishihara's H_1 – H_2 curves relate to the characteristics of the profiles used by Ishihara (1985) to develop the curves and the characteristics of the ground shaking to which these profiles were subjected.

To account for the limiting-crust-thickness phenomenon on the severity of surficial liquefaction manifestations using a more quantitative approach, Maurer et al. (2015a) utilized Ishihara's boundary curves to derive an alternative MSI model, LPI_{ish}

$$LPI_{ish} = \int_{H_1}^{z_{max}} F_{LPI_{ish}}(FS) \cdot \frac{25.56}{z} dz$$
 (2a)

where

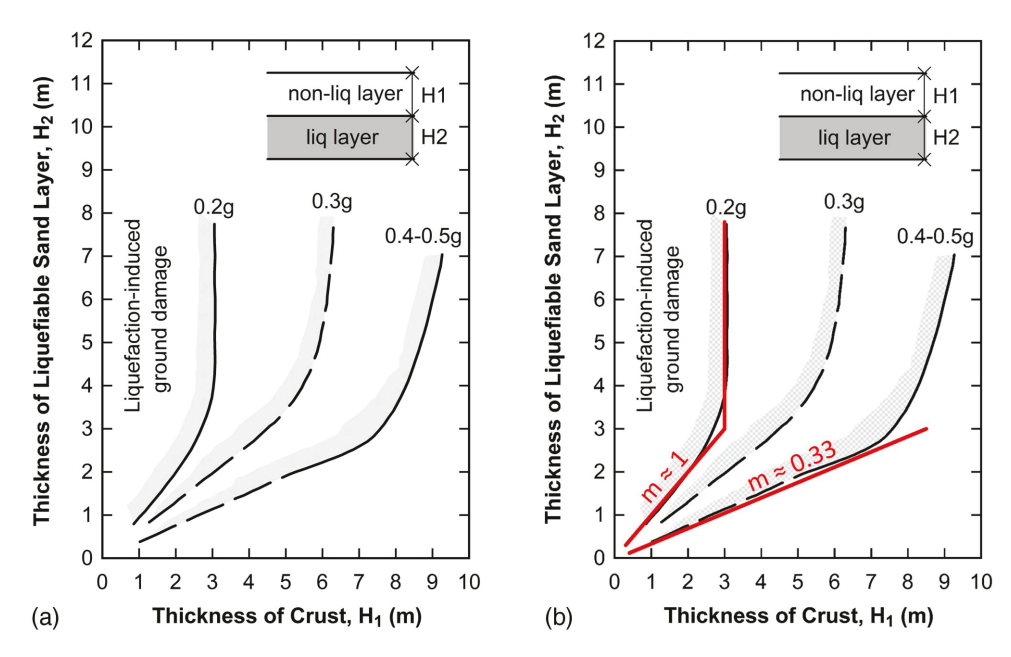


Fig. 1. (a) Ishihara's H_1 – H_2 chart showing the relationship between the thicknesses of the nonliquefiable capping layer (H_1) and underlying liquefiable layer (H_2) for identifying liquefaction-induced damage as a function of PGA (after Ishihara 1985); and (b) Ishihara H_1 – H_2 boundary curves and approximation of the boundary curves by two straight lines.

$$F_{\mathrm{LPI}_{ish}}(FS) = \begin{cases} 1 - FS & \text{if } FS \le 1 \cap H_1 \cdot m(FS) \le 3 \text{ m} \\ 0 & \text{otherwise} \end{cases}$$
 (2b)

and

$$m(FS) = \exp\left[\frac{5}{25.56 \cdot (1 - FS)}\right] - 1;$$
 $m(FS > 0.95) = 100$ (2c)

where FS and z_{max} are defined the same as they are for LPI; and m = slope of the lower portion of the Ishihara $H_1 - H_2$ boundary curve, as shown in Fig. 1(b).

As can be surmised from Eq. (2), the LPI $_{ish}$ framework explicitly accounts for the limiting thickness of the nonliquefied crust by imposing a constraint on $F_{\text{LPI}_{ish}}(FS)$ and uses a power-law depth weighting function, consistent with Ishihara's H_1 – H_2 boundary curves (as discussed in more detail subsequently in regards to the derivation of LSN $_{ish}$). The power-law depth weighting function results in a LPI $_{ish}$ model giving a higher weight to shallower layers than the LPI model in predicting the severity of surficial liquefaction manifestations.

Liquefaction Severity Number

As stated in the "Introduction," LSN was proposed by van Ballegooy et al. (2012, 2014b) and uses the Ishihara and Yoshimine (1992) relationship relating FS, D_r , and ε_v to account for the contractive/dilative tendencies of the soil on the severity of surficial liquefaction manifestations. LSN is given by

$$LSN = \int_0^{z_{\text{max}}} 1,000 \cdot \frac{\varepsilon_v}{z} dz$$
 (3)

where $z_{\rm max}$ = maximum depth considered, generally 10 m, and ε_v is estimated by using the relationship proposed by Zhang et al. (2002) [entered as a decimal in Eq. (3)], which is based on the FS- D_r - ε_v relationship proposed by Ishihara and Yoshimine (1992). Thus, unlike the LPI and LPI $_{ish}$ models, which only consider the influence

of soil strata with FS < 1 on the severity of surficial liquefaction manifestations, the LSN model considers the contribution of layers with $FS \le 2$ via the $FS-D_r-\varepsilon_v$ relationship proposed by Ishihara and Yoshimine (1992).

Derivation of Ishihara-Inspired LSN

As mentioned previously, the LSN_{ish} model merges the positive attributes of the LPI_{ish} and LSN models. The derivation of the LSN_{ish} model follows a procedure similar to the derivation of the LPI_{ish} model (Maurer et al. 2015a) and is detailed in the following subsections.

Assumptions

The following assumptions were used in the derivation:

Assumption 1: All of Ishihara's boundary curves represent the liquefaction response of profiles having similar characteristics. In stress-based simplified liquefaction triggering models, FS is computed as the ratio of normalized cyclic resistance ratio ($CRR_{M7.5}$) to normalized cyclic stress ratio (CSR^*) (i.e., $FS = CRR_{M7.5}/CSR^*$). Because it is assumed that all of the Ishihara's boundary curves represent the liquefaction response of similar profiles, the $CRR_{M7.5}$ corresponding to all of these curves are also similar, which implies that the liquefiable strata (H_2) for the profiles used to develop the boundary curves can be represented by a single normalized penetration resistance. Also, because CSR^* is directly proportional to a_{max} , it follows that FS for the liquefiable strata (H_2) will be inversely proportional to a_{max} .

Assumption 2: Each of Ishihara's H_1-H_2 boundary curves reasonably represents the same value of LSN_{ish} (i.e., the threshold LSN_{ish} value for the occurrence of surficial liquefaction manifestation).

Assumption 3: Each of Ishihara's H_1 – H_2 boundary curves can be approximated by two straight lines, wherein the initial portion of the curve is assumed to have a slope m and the latter portion is approximated as a vertical line having a slope of ∞ , as shown

in Fig. 1(b). As such, the thickness of the liquefiable strata (H_2) , and the thickness of the nonliquefiable crust (H_1) may be related through the slope (m) that is unique to each boundary curve (i.e., $H_2 = H_1 \times m$).

Assumption 4: The liquefiable stratum (H_2) can be represented by a single value of FS.

Functional Form of LSN_{ish}

The functional form of the LSN_{ish} model is

$$LSN_{ish} = \int_{H_1}^{H_1 + H_2} F_{LSN_{ish}}(\varepsilon_v) \cdot w_{LSN_{ish}}(z) dz \tag{4}$$

where $F_{\mathrm{LSN}_{ish}}(\varepsilon_v)$ = contribution of FS and D_r on the severity of surficial liquefaction manifestations via ε_v ; and $w_{\mathrm{LSN}_{ish}}(z)$ = depth weighting function.

Per Assumption 4, the liquefiable stratum can be represented by a single value of FS. Also, per Assumption 1, the normalized penetration resistance of the liquefiable stratum also can be reasonably represented by a given penetration resistance. From these two assumptions, it is implied that the volumetric strain in the liquefiable strata can be represented by a single value of ε_v , and as a result, $F_{\text{LSN}_{ish}}(\varepsilon_v)$ can be taken out of the integral

$$LSN_{ish} = F_{LSN_{ish}}(\varepsilon_v) \int_{H_1}^{H_1 + H_2} w_{LSN_{ish}}(z) dz$$
 (5)

Per Assumption 2, Ishihara's H_1 – H_2 boundary curves reasonably represent the same value of LSN_{ish}, and thus the integral in Eq. (5) must be constant and independent of the values of H_1 and H_2 . This condition is satisfied by assuming a power-law functional form of $w_{\text{LSN}_{ish}}(z)$

$$w_{\text{LSN}_{ish}}(z) = \frac{k}{z} \tag{6}$$

where k = constant that will be determined subsequently. Per Assumption 3, $H_2 = H_1 \times m$. Thus, Eq. (5) can be modified as follows:

$$\begin{split} \mathrm{LSN}_{ish} &= F_{\mathrm{LSN}_{ish}}(\varepsilon_v) \int_{H_1}^{H_1(m+1)} \frac{k}{z} dz \\ &= F_{\mathrm{LSN}_{ish}}(\varepsilon_v) \cdot k \cdot \ln \left(\frac{H_1(1+m)}{H_1} \right) \\ &= F_{\mathrm{LSN}_{ish}}(\varepsilon_v) \cdot k \cdot \ln(m+1) = c \end{split} \tag{7}$$

where c = constant equal to the threshold value of LSN_{ish} for surficial liquefaction manifestation.

Rearranging the terms in Eq. (7), the slope (m) can be expressed

$$m = \exp\left(\frac{c}{k \cdot F_{\text{LSN}_{ich}}(\varepsilon_v)}\right) - 1 \tag{8}$$

Determining Constants

As shown in Eq. (8), a relationship can be established between m and ε_v . Also, from Assumption 1, the FS for the boundary curves associated with $a_{\rm max}$ of 0.2g and 0.4g–0.5g (\sim 0.45g) may be related as follows:

$$\frac{FS_{0.4-0.5g}}{FS_{0.2g}} \approx \frac{0.2g}{0.45g} \Rightarrow FS_{0.45g} = 0.45 \ FS_{0.2g}$$
 (9)

Moreover, the slopes of the initial portion of the boundary curves associated with $a_{\rm max}=0.2g$ and 0.4g–0.5g can be

approximated as 1 and 0.33, respectively [Fig. 1(b)]. Accordingly, from Eq. (8), the slopes of these two boundary curves can be expressed

$$m_{0.2g} = \exp\left(\frac{c}{k \cdot F_{\text{LSN}_{lsh}}(\varepsilon_v)_{0.2g}}\right) - 1 \approx 1 \tag{10}$$

and

$$m_{0.45g} = \exp\left(\frac{c}{k \cdot F_{\text{LSN}_{ich}}(\varepsilon_v)_{0.45g}}\right) - 1 \approx 0.33 \tag{11}$$

where c = threshold values of LSN $_{ish}$ (i.e., the LSN $_{ish}$ value that is expected to segregate cases with and without manifestations). Herein, it is assumed that c=5, similar to the threshold LPI and LPI $_{ish}$ proposed by Iwasaki et al. (1978) and Maurer et al. (2015a), respectively. This value is also the central value that Tonkin and Taylor (2013) used for the LSN criterion for no surficial liquefaction manifestations (i.e., 0 < LSN < 10: "no surficial manifestations" predicted). This choice of c is arbitrary and could be any number that serves as a threshold for distinguishing cases with and without manifestations in forward analyses.

 $F_{\mathrm{LSN}_{ish}}(\varepsilon_v)$ is defined herein as a linear function of ε_v , where ε_v can be estimated using the Zhang et al. (2002) procedure. The Zhang et al. (2002) procedure estimates ε_v as a function of FS and the normalized cone penetration test (CPT) tip resistance (q_{c1Ncs}) and is based on the FS- D_r - ε_v relationship proposed by Ishihara and Yoshimine (1992). The maximum value of ε_v per Ishihara and Yoshimine (1992) is 5.5%. Because it is desired that $F_{\mathrm{LSN}_{ish}}(\varepsilon_v)$ ranges from 0 to 1 (to be consistent with the ranges of F_{LPI} and $F_{\mathrm{LPI}_{ish}}$ parameters in the LPI and LPI_{ish} models, respectively), $F_{\mathrm{LSN}_{ish}}(\varepsilon_v)$ is expressed

$$F_{\text{LSN}_{ish}}(\varepsilon_v) = \frac{\varepsilon_v}{5.5} \tag{12}$$

where ε_v is expressed as a percent. To determine the value of k that satisfies Eqs. (10) and (11), representative values of FS and q_{c1Ncs} need to be estimated.

As stated previously, Ishihara (1985) developed the H_1 – H_2 chart [Fig. 1(a)] from data from two earthquakes, the 1983 $M_{\rm w}$ 7.7 Nihonkai-Chubu earthquake in Japan and the 1976 $M_{\rm w}$ 7.8 Tangshan earthquake in China. For the liquefaction case histories from the Nihonkai-Chubu earthquake, Ishihara (1985) stated that the liquefied deposits were subjected to peak ground accelerations of approximately 0.2g and had standard penetration test (SPT) N-values less than or equal 10 blows/30 cm.

For the liquefaction case histories from the Tangshan earthquake, Ishihara (1985) stated that the liquefied deposits were subjected to peak ground accelerations of 0.4g to 0.5g and had N-values ranging from 5 to 24 blows/30 cm, but most were less than N = 20 blows/30 cm. No information was given by Ishihara (1985) regarding whether these blow counts are normalized/ corrected for vertical effective confining stress, hammer energy, rod length, sampler configuration, influence of fines content, or other factors. With no further guidance, it is assumed that N =10 blows/30 cm is representative of the uncorrected SPT penetration resistance for the liquefiable stratum (H_2) for all the curves. Correcting this value for depths corresponding to the center of H_2 and making further adjustments to account for typical rig and sampler configurations in the US versus Japan (e.g., Kovacs and Salomone 1984), the representative normalized SPT penetration resistance (i.e., $N_{1.60cs}$) for the liquefiable stratum (H_2) is estimated to be approximately 14.5 blows/30 cm, which corresponds to $q_{c1Ncs} \approx 103$ (e.g., Ulmer et al. 2020). For this value of q_{c1Ncs} and for Eqs. (10) and (11) to be satisfied, $FS_{0.2g} \approx 0.99$ and $k \approx 36.929$.

Final Form

The final form of the LSN_{ish} model is

$$LSN_{ish} = \int_{H_1}^{z_{max}} F_{LSN_{ish}}(\varepsilon_v) \cdot \frac{36.929}{z} \cdot dz$$
 (13a)

where $z_{\rm max}$ is defined the same as it is for LPI (e.g., 20 m), and

$$F_{\mathrm{LSN}_{lsh}}(\varepsilon_v) = \begin{cases} \frac{\varepsilon_v}{5.5} & \text{if } FS \leq 2 \quad \text{and} \quad H_1 \cdot m(\varepsilon_v) \leq 3 \text{ m} \\ 0 & \text{otherwise} \end{cases}$$
 (13b)

$$m(\varepsilon_v) = \exp\left(\frac{0.7447}{\varepsilon_v}\right) - 1; \qquad m(\varepsilon_v < 0.16) = 100 \quad (13c)$$

where ε_v is expressed as a percent. As can be surmised from Eq. (13), the LSN_{ish} model explicitly accounts for (1) the influence of ε_v on the severity of surficial liquefaction manifestations; (2) the limiting-crust-thickness phenomenon; and (3) the contribution of liquefiable layers with $FS \leq 2$ to the severity of surficial liquefaction manifestations.

Specific to the second point mentioned in the preceding sentence, the limiting crust thickness is accounted for in the LSN_{ish} model via the requirement that $H_1 \cdot m(\varepsilon_v) \leq 3$ m in Eq. (13b). Because m is a function of ε_v (which in turn is a function of normalized penetration resistance and FS), it is implied that as ε_v increases, the thickness of the nonliquefiable crust required to suppress manifestations increases. Fig. 2 illustrates the limiting-crust-thickness criterion inherent to the LSN_{ish} model in H_1 – H_2 space.

The limiting crust thickness is equal to 3 m/m, where m is a function of the penetration resistance of the soil (e.g., q_{c1Ncs}) and FS against liquefaction triggering (i.e., if H_1 is greater than this limiting crust thickness, liquefaction manifestations are not

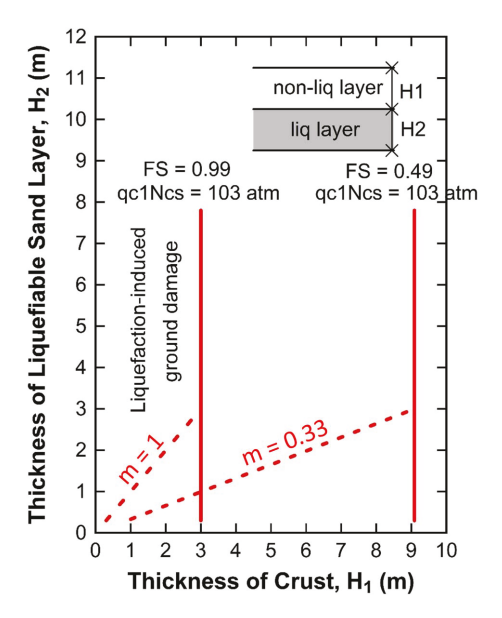


Fig. 2. Limiting thickness of the nonliquefiable crust/capping layer criterion inherent to the LSN_{ish} model in $H_1 - H_2$ space. The two limiting thicknesses shown (solid vertical lines) are for $q_{c1Ncs} = 103$ and FS = 0.99, and $q_{c1Ncs} = 103$ and FS = 0.49, which approximately correspond to Ishihara's boundary curves for 0.2g and 0.4g–0.5g.

predicted regardless of the thickness and other liquefaction response characteristics of H_2). The two limiting crust thicknesses shown in Fig. 2 (vertical solid lines) are for $q_{c1Ncs}=103$ and FS=0.99, and $q_{c1Ncs}=103$ and FS=0.49, which approximately correspond to Ishihara's boundary curves for 0.2g and 0.4g-0.5g, respectively. The difference between the curves shown in Fig. 2 and Ishihara's boundary curves [Fig. 1(a)] is most pronounced when $H_2 < 3$ m, where Ishihara's curves vary the limiting crust thickness as a function of H_2 but the LSN $_{ish}$ model does not. However, the variation of the limiting crust thickness as a function of H_2 for cases when $H_2 < 3$ m is captured by other attributes of the LSN $_{ish}$ model, as illustrated in the following.

Eq. (13) is applied to simple two-layer profiles composed of layers H_1 and H_2 , the same as those used by Ishihara (1985). The thickness of the nonliquefiable layer (H_1) is defined by the depth of the groundwater table, and the liquefiable layer (H_2) is assumed to have a representative penetration resistance of $q_{c1Ncs} \approx 103$ atm. The profiles are subjected to earthquake motions from an M_w 7.75 event with $a_{max} = 0.2g$ [M_w 7.75 is the average of the magnitudes of the Nihonkai-Chubu and Tangshan earthquakes used by Ishihara (1985) to derive his boundary curves]. The LSN $_{ish}$ values are computed using Eq. (13) in conjunction with the Boulanger and Idriss (2014, 2016) (BI14) CPT-based simplified liquefaction triggering model.

As may be observed in Fig. 3, the Ishihara $0.2g\,H_1-H_2$ boundary curve is a reasonable contour for LSN_{ish} = 5, the threshold value for surficial liquefaction manifestations assumed in the derivation of Eq. (13). The slight deviation to this is for thicker liquefiable layers (i.e., $H_2 \ge 5$ m), which stems from the assumptions that the entire liquefiable stratum can be represented by a single value of q_{c1Ncs} and a single value of FS; these assumptions become less valid as H_2 increases.

The benefit of using the LSN_{ish} model over the Ishihara H_1 – H_2 boundary curves is for profiles that cannot be reasonably represented by two layers, where the penetration resistance of the lique-fiable soil is not represented by $q_{c1Ncs} \approx 103$, and/or for scenarios

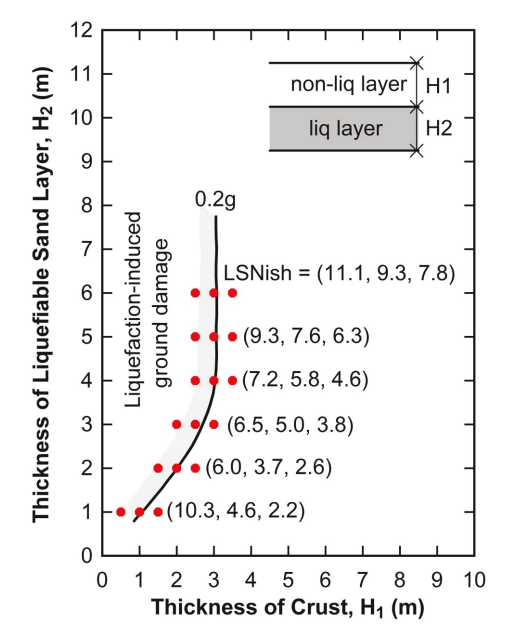


Fig. 3. Ishihara's H_1 – H_2 curve for 0.2g and LSN_{ish} values computed using Eq. (13) in conjunction with the BI14 simplified triggering model for a simple two-layer profile having varying thicknesses for H_1 and H_2 and $q_{c1Ncs} \approx 103$ atm for H_2 .

where the earthquakes have magnitudes that differ from M_w 7.7–7.8. Eq. (13) is applied to such a scenario in Fig. 4 where a soil profile is analyzed for shaking from an M_w 7.0 event with $a_{\rm max}=0.15g$. Based on the Soil Behavior Type Index (I_c) (Robertson and Wride 1998), the profile is mostly composed of clean sand to silty sand below the groundwater table, with the exception of a very thin clayey silt to silty clay layer at a depth of ~4.75 m [Fig. 4(b)]. However, the penetration resistance of the clean sand to silty sand increases somewhat significantly with depth [Fig. 4(a)].

As shown in Fig. 4(c), the FS computed using the BI14 triggering model is mostly slightly greater than 1 between depths of 4.5–9.3 m and mostly less than 2 for depths between 9.3 and 14 m. Because FS > 1 for all but a very few depths, the computed values for LPI and LPI_{ish} are approximately zero. However, because FS ranges between ~ 1 and 2 over a large depth range, LSN and LSN_{ish} are expected to be greater than zero. As a result, this

example can illustrate the difference between LSN and LSN $_{ish}$, specifically the depths that are predicted by each model to contribute to the severity of surficial liquefaction manifestations. Toward this end, two specific depths are considered, 5.52 and 7.51 m.

At depths of 5.52 and 7.51 m, $q_{c1Ncs} = 69.22$ and 92.03 [Fig. 4(a)], respectively, and the corresponding computed FS values are 0.916 and 1.024 [Fig. 4(c)], respectively. Because the FS <2 at both of these depths, both depths are predicted to contribute to the severity of surficial liquefaction manifestations per the LSN model, as indicated by the nonvertical slope of the LSN profile at these depths in Fig. 4(d). However, this is not the case for the LSN_{ish} model, where only the liquefaction response of the soil at a 5.52 m depth is considered to contribute to surficial manifestations, as indicated by the nonvertical slope of the LSN_{ish} profile at a depth of 5.52 m and a vertical slope of the LSN_{ish} profile at 7.51 m in Fig. 4(d).

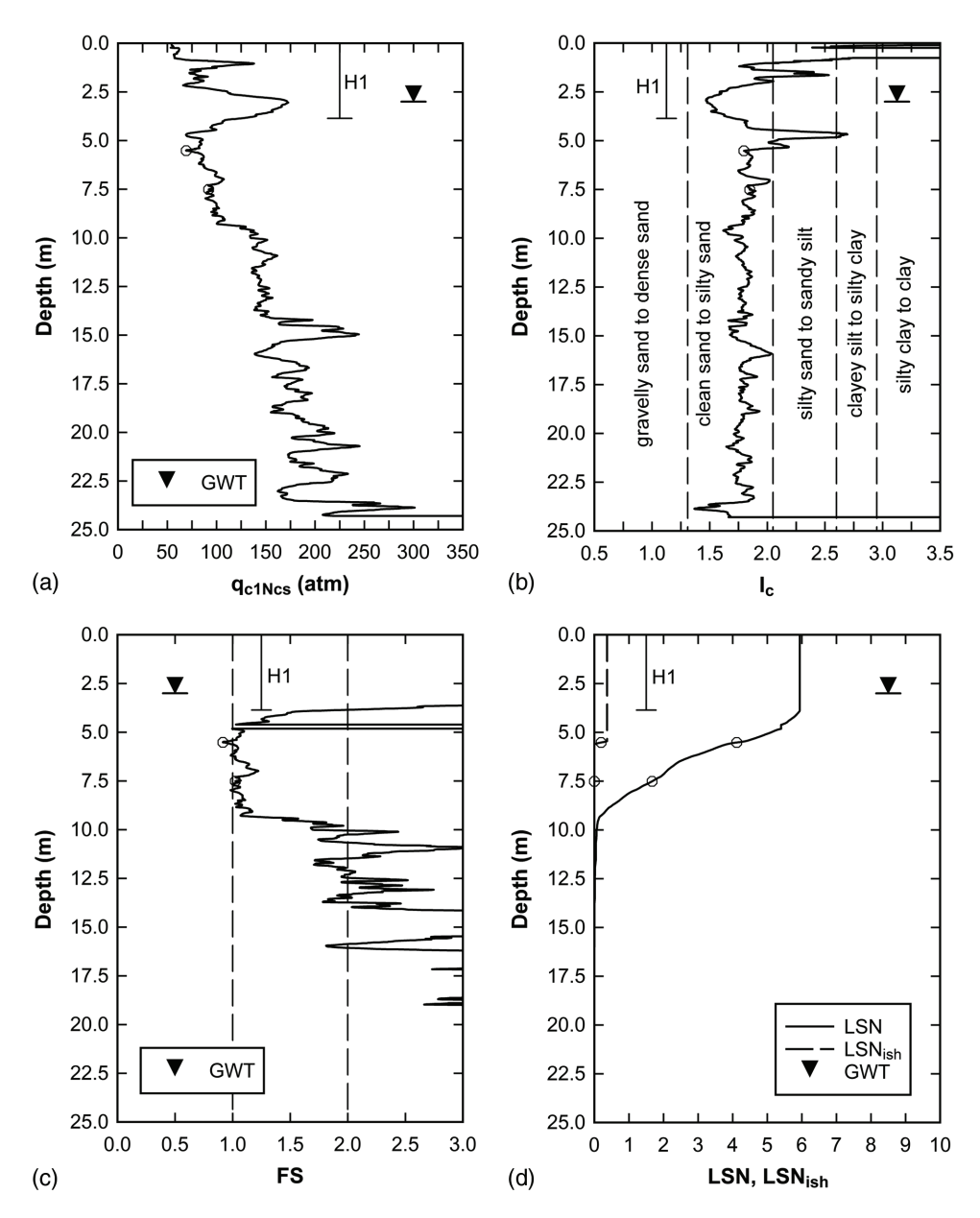


Fig. 4. Example illustrating the implementation of the LSN_{ish} model for an actual soil profile subjected to shaking from an M_w 7.0 earthquake and an $a_{max} = 0.15g$, with emphasis on the differences in the contributions to surficial liquefaction manifestations at two depths: (a) normalized CPT tip resistance q_{c1Ncs} ; (b) soil behavior type index Ic; (c) FS against liquefaction triggering per BI14; and (d) comparison between LSN and LSN_{ish}.

The reason for this is that m=0.352 and 1.364 at depths of 5.52 and 7.51 m, respectively. As a result, the limiting crust thicknesses for the soils at 5.52 and 7.51 m depths are ~ 8.5 and 2.2 m, respectively; if H_1 is greater than the limiting thickness, then the liquefaction response of the soil at that depth is not predicted to contribute to surficial manifestations in the LSN_{ish} model. For this scenario, $H_1=3.86$ m (i.e., the shallowest depth below the groundwater table, where the FS < 2 and $I_c \le 2.6$). Accordingly, the liquefaction response of the soil at the depth of 5.52 m is predicted to contribute to surficial liquefaction manifestation, but not the soil at a depth of 7.51 m.

Evaluation of MSI Models

Canterbury Earthquakes Liquefaction Case-History Data Set

The LPI, LPI_{ish}, LSN, and LSN_{ish} models were evaluated using 7,167 CPT liquefaction case histories from the 2010-2011 Canterbury earthquake sequence and the 2016 Valentine's Day earthquake, collectively referred to henceforth as the Canterbury earthquakes (CE). These 7,167 CPT liquefaction case histories were derived as a subset of approximately 10,000 well-documented case histories resulting from the M_w 7.1 September 2010 Darfield, M_w 6.2 February 2011 Christchurch, and the M_w 5.7 February 2016 Valentine's Day earthquakes in Canterbury, New Zealand, largely assembled by Maurer et al. (2014, 2015d, c, b, 2017a, b, 2019) and Geyin et al. (2021). The case histories consist of classifications of liquefaction manifestations, geotechnical and hydrological data, and ground-motion intensity measures. The severity of the liquefaction manifestations was based on postevent observations and high-resolution aerial photographs and satellite imagery taken within a few days after the earthquakes.

None of the MSI models being evaluated account for the influence of nonliquefiable, high-FC, high-plasticity interbedded soil strata on the occurrence/severity of surficial liquefaction manifestations. Therefore, the MSI models can be best evaluated using case histories comprised predominantly clean to nonplastic silty sand profiles. Maurer et al. (2015d) found that sites in the region that have an average I_c for the upper 10 m of the soil profile (I_{c10}) less than 2.05 generally correspond to sites having predominantly clean to nonplastic silty sands. Accordingly, the 7,167 liquefaction case histories used in this study only comprised CPT soundings that have $I_{c10} < 2.05$; the locations of the CPT soundings for these case histories are shown in Fig. 5.

Of the 7,167 case histories, 2,574 cases are from the 2010 Darfield earthquake, 2,582 cases are from the 2011 Christchurch earthquake, and 2,011 cases are from the 2016 Valentine's Day earthquake. Furthermore, 38% of the case histories were categorized as no manifestation, and the remaining 62% were categorized as either marginal, moderate, or severe manifestations following the Green et al. (2014) classification (Fig. S1 and Table S1).

Values for $a_{\rm max}$ are needed to estimate the seismic demand at the case history sites. In prior CE studies (e.g., Green et al. 2011, 2014; Maurer et al. 2014, 2015a, b, c, d, 2017a, b, 2019; van Ballegooy et al. 2015; among others), $a_{\rm max}$ values were obtained using the Bradley (2013b) procedure, which combines the unconditional $a_{\rm max}$ distributions as estimated by the Bradley (2013a) ground motion prediction equation, the actual recorded $a_{\rm max}$ values at the strong motion stations (SMS), and the spatial correlation model of Goda and Hong (2008) to compute the conditional $a_{\rm max}$ values at the sites of interest.

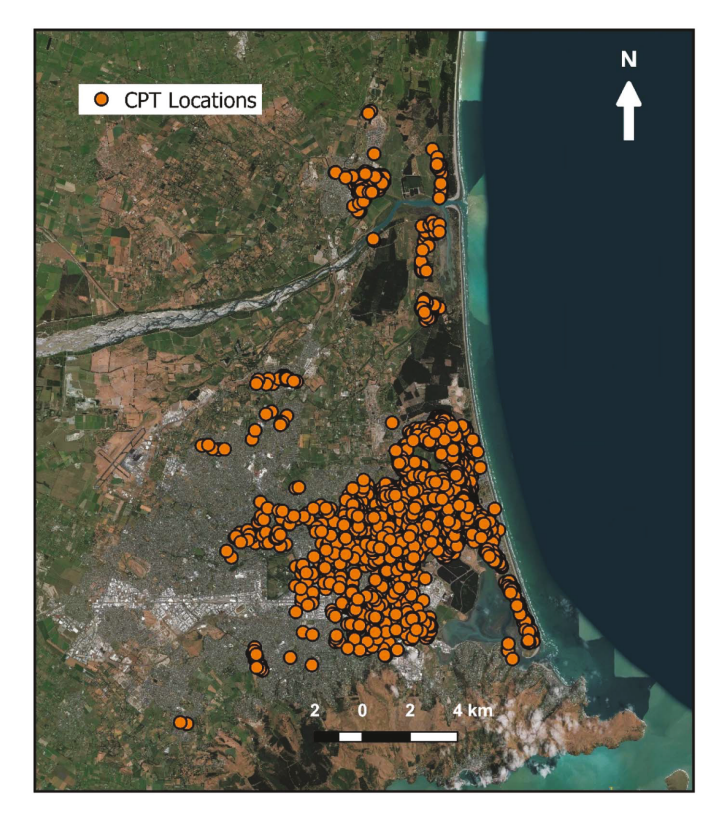


Fig. 5. Map of spatial distributions of CPT sounding locations from CE. (Microsoft Bing screenshot reprinted with permission from Microsoft Corporation, base image data © 2021 Microsoft Corporation, Earthstar Geographics SIO.)

However, the recorded $a_{\rm max}$ values at four SMSs during the ${\rm M_w}$ 6.2 February 2011 Christchurch earthquake were inferred to be associated with high-frequency dilation spikes as a result of liquefaction triggering and were higher than the preliquefaction $a_{\rm max}$ values (e.g., Wotherspoon et al. 2014, 2015). Such artificially high $a_{\rm max}$ values at the liquefied SMSs can potentially result in overestimated $a_{\rm max}$ values at the nearby case-history sites (hence, overly conservative seismic demand), which in turn can lead to overpredictions of the severity of surficial liquefaction manifestations (Upadhyaya et al. 2019). Accordingly, in the present study, preliquefaction $a_{\rm max}$ values at the four liquefied SMS were used to estimate $a_{\rm max}$ values at the case history locations for the 2011 Christchurch earthquake. For the 2010 Darfield and 2016 Valentine's Day earthquakes, previously estimated $a_{\rm max}$ values remain unchanged.

Accurate estimation of groundwater table (GWT) depth is critical to liquefaction triggering evaluations. The GWT depth at each case-history site immediately prior to the earthquake was estimated using the robust event-specific regional groundwater models of van Ballegooy et al. (2014a), as in prior CE studies (e.g., Maurer et al. 2014, 2015d, c, a, 2017a, b, 2019; van Ballegooy et al. 2015; Upadhyaya et al. 2018; among others).

Evaluation of Liquefaction Triggering and Severity of Surficial Liquefaction Manifestation

In evaluating the MSI models, FS is used as an input parameter. In the present study, FS was computed using the BI14 CPT-based liquefaction triggering model, although the triggering model proposed by Green et al. (2019) was also used and the results are similar to those presented subsequently for the BI14 model. Inherent to

this process, soils with $I_c > 2.5$ were considered to be nonliquefiable (Maurer et al. 2017b, 2019). Additionally, the FC required to compute q_{c1Ncs} was estimated using the Christchurch-specific I_c -FC correlation proposed by Maurer et al. (2019).

For each CE case history, the predictive efficacies of the LPI, LPI_{ish} , LSN, and LSN_{ish} models were compared by performing receiver operating characteristic (ROC) analyses on the CE data set. An overview of ROC analysis is presented in the following section.

Overview of ROC Analysis

ROC analysis is widely used to evaluate the performance of diagnostic models, including extensive use in medical diagnostics (e.g., Zou 2007) and to a much lesser degree in geotechnical engineering (e.g., Oommen et al. 2010; Maurer et al. 2015d, c, b, 2017a, b, 2019; Green et al. 2017; Zhu et al. 2017; Upadhyaya et al. 2018, 2021). In particular, in cases where the distribution of positives (e.g., cases of observed surficial liquefaction manifestations) and negatives (e.g., cases of no observed surficial liquefaction manifestations) overlap [e.g., Fig. 6(a)], ROC analyses can be used to (1) identify the optimum diagnostic threshold (e.g., LSN_{ish} threshold); and (2) assess the relative efficacy of competing diagnostic models, independent of the thresholds used.

A ROC curve is a plot of the true positive rate ($R_{\rm TP}$) (i.e., surficial liquefaction manifestations were observed, as predicted) versus the false positive rate ($R_{\rm FP}$) (i.e., surficial liquefaction manifestations are predicted, but were not observed) for varying threshold values (e.g., LSN_{ish}). A conceptual illustration of ROC analysis, including the relationship among the distributions for positives and negatives, threshold value, and ROC curve, is shown in Fig. 6.

In ROC curve space, a diagnostic test that has no predictive ability (i.e., a random guess) results in a ROC curve that plots as a 1:1 line through the origin. In contrast, a diagnostic test that has a perfect predictive ability (i.e., a perfect model) plots along the left vertical and upper horizontal axes, connecting at the point (0,1) and indicates the existence of a threshold value that perfectly segregates the data set (e.g., all cases with observed surficial manifestations will have LSN $_{ish}$ above the threshold, and all cases with no observed surficial manifestations will have LSN $_{ish}$ below the threshold).

The area under the ROC curve (AUC) can be used as a metric to evaluate the predictive performance of a diagnostic model (e.g., LSN_{ish} model), whereby a higher AUC value indicates better predictive capabilities (e.g., Fawcett 2005). As such, a random guess returns an AUC of 0.5, whereas a perfect model returns an AUC of 1. The optimum operating point (OOP) in a ROC analysis is defined as the threshold value (e.g., threshold LSN_{ish}) that minimizes the rate of misprediction [i.e., $R_{\rm FP}+(1-R_{\rm TP})$]. Contours of the quantity $[R_{\rm FP}+(1-R_{\rm TP})]$ are isoperformance lines joining points of equivalent performance in ROC space, as illustrated in Fig. 6(b).

Results and Discussion

ROC analyses were performed on the CE data set using the four MSI models (i.e., LPI, LPI_{ish}, LSN_{ish}, and LSN models). ROC statistics (i.e., AUC and OOP) were obtained to evaluate the performance of each MSI model in distinguishing (1) cases with no manifestation from cases with any manifestation severity (Case a); (2) cases with no manifestations from cases with marginal manifestations (Case b); (3) cases with marginal manifestations from cases with moderate manifestations (Case c); and (4) cases with moderate manifestations from cases with severe manifestations (Case d). Table 1 summarizes the ROC statistics (i.e., AUC and OOP) for each MSI model, used in conjunction with the BI14 deterministic triggering model, for different severities of surficial liquefaction manifestations as described previously.

Fig. 7(a) shows the ROC curves for the four different MSI models, considering only the binomial predictive ability (i.e., Case a, cases with no manifestation from cases with any manifestation severity), evaluated in conjunction with the BI14 deterministic triggering model. Also shown in Fig. 7(a) are the optimum threshold values associated with each MSI model. Moreover, Fig. 8(a) compares the AUCs associated with these four different MSI models, evaluated in conjunction with the BI14 deterministic triggering model.

The results from ROC analyses show that the AUC values returned by the four different MSI models follow the order: LPI \approx LPI $_{ish}$ > LSN \approx LSN $_{ish}$. As such, two main observations can be made. First, despite accounting for the limiting-crust-thickness phenomenon, LPI $_{ish}$ and LSN $_{ish}$ did not show improvements over LPI and LSN, respectively. This is likely due to the fact that the case histories used in this study only comprised CPT soundings that have I_{c10} < 2.05, the majority of which are located

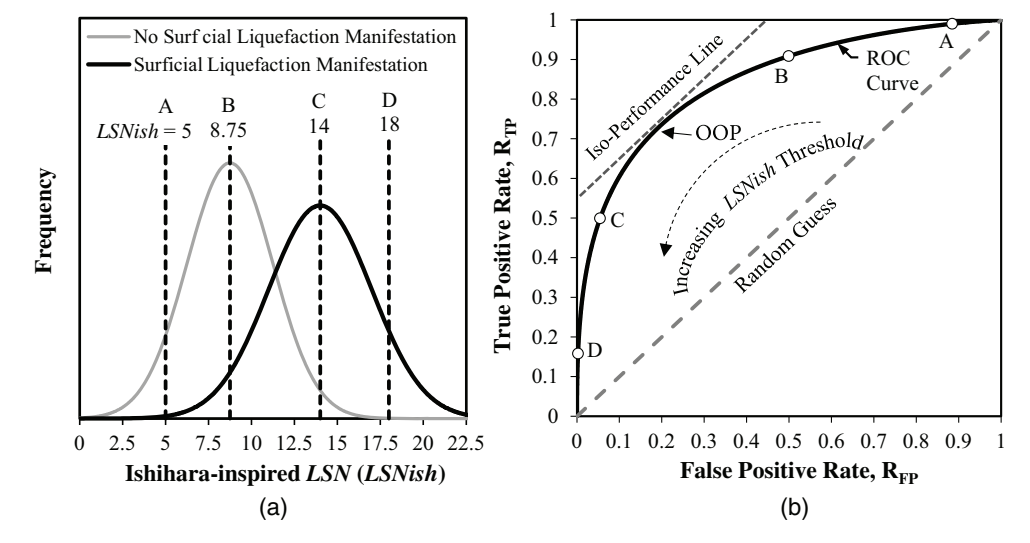


Fig. 6. Conceptual illustration of ROC analyses: (a) frequency distributions of surficial liquefaction manifestation and no surficial liquefaction manifestation observations as a function of LSN_{ish}; and (b) corresponding ROC curve (after Maurer et al. 2015d, c, b).

Table 1. Summary of ROC statistics for different MSI models evaluated using the BI14 deterministic CRR_{M7.5} curve considering different severities of surficial liquefaction manifestation

	Any manifestation		Marginal		Moderate		Severe	
MSI model	AUC	OOP	AUC	OOP	AUC	OOP	AUC	OOP
LPI	0.8500	3.7	0.7893	2.0	0.6852	5.6	0.6839	14.1
LPI_{ish}	0.8473	1.7	0.7868	1.1	0.6821	3.6	0.6926	9.7
LSN	0.7975	10.5	0.7417	9.1	0.6484	15.5	0.6726	24.7
LSN _{ish}	0.8007	5.4	0.7437	5.4	0.6508	7.9	0.6776	16.4

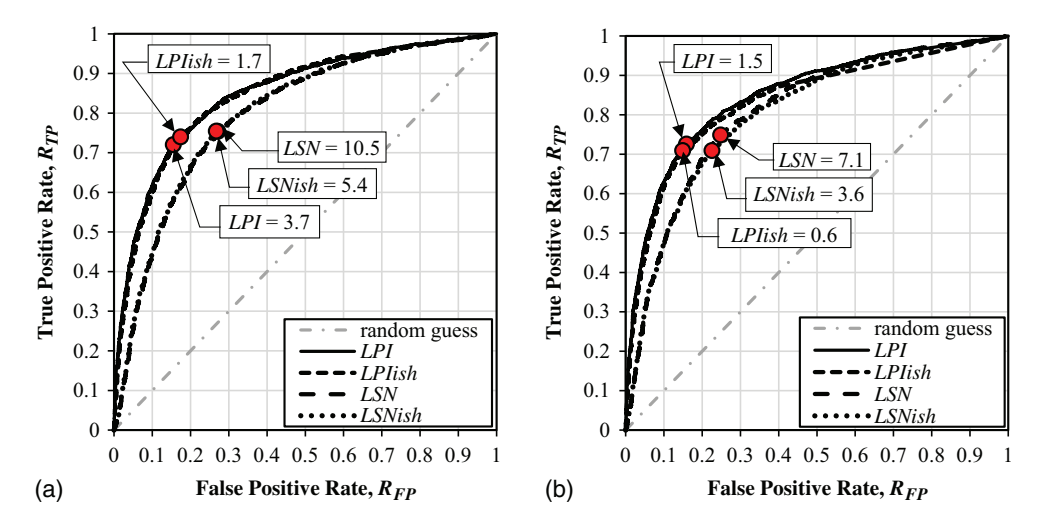


Fig. 7. ROC curves for LPI, LPI $_{ish}$, LSN, and LSN $_{ish}$ models evaluated using: (a) BI14 deterministic CRR $_{M7.5}$; and (b) BI14 median CRR $_{M7.5}$. Also shown are the optimal thresholds for each model.

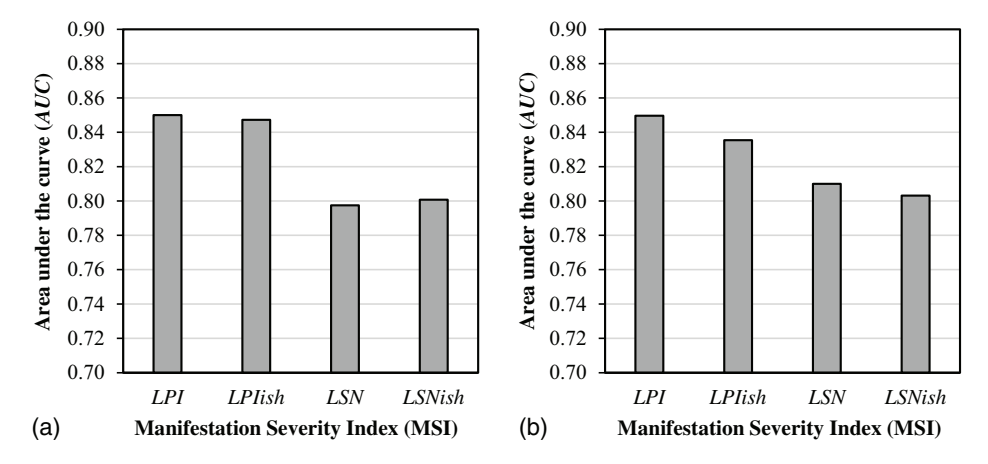


Fig. 8. Comparison of AUC values for the LPI, LPI_{ish}, LSN, and LSN_{ish} models evaluated using: (a) BI14 deterministic $CRR_{M7.5}$; and (b) BI14 median $CRR_{M7.5}$.

in eastern Christchurch (Fig. 5) where the groundwater table is shallow (usually ranging between \sim 1 and 2 m). As a result, the limiting-crust-thickness phenomenon may not have much of an influence on the severity of surficial liquefaction manifestations. Another possible reason could be that Ishihara's H_1 – H_2 boundary curves may not sufficiently represent the influence of nonliquefied crust thickness on the occurrence and severity of manifestations, although the authors believe that the general trends exhibited by Ishihara's H_1 – H_2 boundary curves are correct (e.g., Green et al. 2018).

Second, the higher AUCs for the LPI and LPI $_{ish}$ models than the LSN and LSN $_{ish}$ models indicate that the latter group performs more poorly despite accounting for the influence of soil density on the occurrence/severity of surficial liquefaction manifestation via the FS- D_r - ε_v relationship, contrary to what would be expected. Several factors may explain the cause of the reduced efficacy of these models. For example, the ε_v model of Zhang et al. (2002) is based on the FS- D_r - ε_v relationship proposed by Ishihara and Yoshimine (1992) developed using laboratory test data for reconstituted clean sand samples. In contrast to the FS determined from

Table 2. Summary of ROC statistics for different MSI models evaluated using the BI14 median $CRR_{M7.5}$ curve considering different severities of surficial liquefaction manifestation

MSI model	Any manifestation		Marginal		Moderate		Severe	
	AUC	OOP	AUC	OOP	AUC	OOP	AUC	OOP
LPI	0.8496	1.5	0.7873	1.0	0.6872	3.4	0.6840	7.4
LPI_{ish}	0.8354	0.6	0.7688	0.3	0.6811	1.2	0.6880	4.6
LSN	0.8100	7.1	0.7525	7.5	0.6596	10.3	0.6809	23.2
LSN _{ish}	0.8031	3.6	0.7421	2.6	0.6607	5.3	0.6853	13.3

laboratory tests for a specific soil that has a specific fabric, the field-based triggering curves are developed from a range of soils having a range of fabrics. As a result, there may be inconsistencies in how the Ishihara and Yoshimine (1992) $FS-D_r-\varepsilon_v$ relationship is being applied in conjunction with FS determined from triggering models based on field case histories.

However, the most likely reason for the poorer performance of the LSN and LSN $_{ish}$ models is that the influence of posttriggering volumetric strain potential of medium-dense to dense soils on the severity of surficial liquefaction manifestations is being double-counted by these models. This is because FS, which is used as an input to compute ε_v , inherently accounts for such effects via the shape of the $CRR_{M7.5}$ curve. Specifically, the $CRR_{M7.5}$ curves likely tend toward vertical at medium to high penetration resistance due to dilative tendencies of medium-dense to dense soils that inhibit the surficial liquefaction manifestation, even if liquefaction is triggered at depth (e.g., Dobry 1989).

Although the existing triggering curves are treated as actual or true triggering curves in current practice, in reality they are combined triggering and manifestation curves. This is mainly because the $CRR_{M7.5}$ curves are based on the liquefaction response of profiles inferred from postearthquake surface observations at sites. Sites without surficial evidence of liquefaction are classified, by default, as no liquefaction, despite the possibility of liquefaction having been triggered at depth, but not manifesting at the ground surface. Consequently, embedded in the resulting triggering curve are factors that relate not only to triggering, but also to posttriggering surface manifestation.

These findings suggest that the current models for predicting liquefaction response may not account for the mechanics of liquefaction triggering and surface manifestation in a consistent and sufficient manner. The liquefaction triggering and manifestation models need to be developed simultaneously within a consistent framework that provides a clear separation and proper accounting of mechanics controlling each phenomenon. Given that the LSN_{ish} model accounts for the factors controlling manifestation in a more appropriate manner, it is hypothesized that the LSN_{ish} model would result in better predictions of the severity of surficial liquefaction manifestation than the other MSI models examined herein, if used in conjunction with a true liquefaction triggering curve (i.e., free of factors influencing surficial liquefaction manifestation) (Upadhyaya 2019). As detailed by Upadhyaya (2019), one approach for doing this is to group the liquefaction case histories based on the severity of surficial liquefaction manifestations and assigning the groups severity indices. Then, CSR* for the case histories, in conjunction with an MSI model, can be used to backcalculate a triggering curve (i.e., CRR_{M7.5} curve) that removes the influence of surficial manifestations.

Finally, several studies have proposed using median $CRR_{M7.5}$ curves to compute the FS (e.g., Cetin et al. 2018). The reason for this is that deterministic $CRR_{M7.5}$ curves are almost always conservatively positioned to minimize the number of false negatives (i.e., liquefaction cases that fall below or to the right of the $CRR_{M7.5}$

curve, with the positioning of the BI14 deterministic $CRR_{M7.5}$ curve corresponding to a probability of liquefaction of 15%). As a result, FS computed using the deterministic $CRR_{M7.5}$ curve may lead to conservative predictions. For unbiased estimates of FS, use of median $CRR_{M7.5}$ may be more appropriate. However, using the median $CRR_{M7.5}$ curve to compute MSI values and comparing them with established MSI severity thresholds based on case histories analyzed using FS computed using deterministic $CRR_{M7.5}$ curves is inconsistent with the way the MSI severity thresholds were established and therefore introduces unquantified bias. Nevertheless, FS were computed using the median BI14 $CRR_{M7.5}$ curve and used to compute the MSI indices.

Figs. 7(b) and 8(b) illustrate the ROC analyses, and Table 2 summarizes the ROC statistics (i.e., AUC and OOP) for each MSI model used in conjunction with the BI14 median triggering model for different severities of surficial liquefaction manifestations as described previously.

It can be seen that the AUCs for the LPI and LPI_{ish} models are generally slightly higher when evaluated in conjunction with the deterministic triggering model than with the median triggering model. In contrast, the AUCs for LSN and LSN_{ish} models are generally slightly lower when evaluated using the deterministic model than using the median CRR_{M7.5} model. Because the changes in AUC are not very significant between the deterministic and median models, it can be inferred that the MSI models are equally efficacious using either variant of the CRR_{M7.5} curves. However, the optimal threshold MSI values are different between the deterministic and median triggering models, with the median model resulting in lower threshold values than the deterministic model.

For example, the optimal threshold LSN $_{ish}$ values distinguishing cases of no manifestations from cases with any manifestation severity when evaluated using the deterministic and median CRR $_{M7.5}$ curves are 5.4 and 3.6, respectively. This is consistent with the preceding comment that using the median CRR $_{M7.5}$ curve to compute MSI values and comparing them with established MSI severity thresholds based on case histories analyzed using FS computed using deterministic CRR $_{M7.5}$ curves introduces bias and is viewed by the authors as being inappropriate.

Conclusion

This paper assesses the limitations of surface liquefaction manifestation severity index models that are used in conjunction with simplified stress-based triggering models. Specifically, three existing MSI models are evaluated (i.e., LPI, LPI_{ish}, and LSN models) and a fourth MSI model is developed and evaluated (i.e., LSN_{ish}). These models account for various factors influencing the severity of surficial liquefaction manifestations, with the LSN_{ish} model accounting for more factors than the others.

The LSN_{ish} model was derived as a conceptual merger of the LSN formulation and Ishihara's H_1 – H_2 boundary curves. As such, LSN_{ish} conceptually accounts for (1) the influence of

postliquefaction volumetric strain potential on the severity of surficial liquefaction manifestation; (2) the limiting-crust-thickness phenomenon, where a nonliquefied capping stratum having an equal or greater thickness than the limiting crust thickness inhibits any surficial liquefaction manifestations regardless of the liquefaction response of the underlying strata; and (3) the contribution of layers where liquefaction did not trigger (i.e., FS > 1), but the excess pore pressures due to shaking are sufficiently high enough to potentially contribute to surficial manifestations.

The predictive efficacies of the four MSI models were evaluated using 7,167 well-documented CPT liquefaction case histories from the 2010–2011 Canterbury earthquake sequence and the 2016 Valentine's Day earthquake; the case histories comprised predominantly clean to nonplastic silty sand profiles. These models were evaluated in conjunction with the BI14 triggering model, where both the deterministic and median $CRR_{M7.5}$ curves were used to compute FS. It was observed that the predictive efficacies of LSN_{ish} and LSN models were lower than those of LPI and LPI_{ish}, despite the former two MSI models accounting for the additional influence of soil density on the severity of surficial liquefaction manifestation via the $FS-D_r-\varepsilon_r$ relationship.

The likely reason for this is that the influence of posttriggering volumetric strain potential on the severity of surficial liquefaction manifestation is being double-counted by the LSN and LSN_{ish} models because the shape of the $CRR_{M7.5}$ curve inherently accounts for the dilative tendencies of medium-dense to dense soils, which inhibit surficial liquefaction manifestations even when liquefaction is triggered at depth. These findings suggest that current frameworks for predicting the occurrence/severity of surficial liquefaction manifestation do not account for the mechanics of triggering and manifestation in a proper and sufficient manner. Although the triggering curves are assumed to be true (i.e., free of factors influencing manifestation), in reality they inherently account for some of the factors controlling surficial manifestation of liquefaction, particularly for denser soils. Thus, there is a need to develop a framework that consistently and appropriately accounts for the mechanics behind liquefaction triggering and surficial liquefaction manifestation (e.g., Upadhyaya 2019).

Finally, because several studies have proposed using median $CRR_{M7.5}$ curves to compute the FS against liquefaction triggering, we repeated our assessment of the efficacies of the MSI models using median CRR_{M7.5} curves. The efficacies of the LPI and LPI_{ish} models were generally slightly higher when evaluated in conjunction with the deterministic $CRR_{M7.5}$ curve than with the median CRR_{M7.5} curve. In contrast, the efficacies of the LSN and LSN_{ish} models were generally slightly lower when evaluated using the deterministic CRR_{M7.5} curve than using the median $CRR_{M7.5}$ curve. However, the differences in the efficacies are not very significant between the deterministic and median CRR_{M7.5} curves, and it can be inferred that the MSI models perform equally well using either variant of the CRR_{M7.5} curves. However, the optimal threshold MSI values are different between the deterministic and median $CRR_{M7.5}$ curves. This implies that using the median CRR_{M7.5} curve to compute MSI values and comparing them with established MSI severity thresholds based on case histories analyzed using FS computed using deterministic CRR_{M7.5} curves introduces an unquantified bias.

Data Availability Statement

The Canterbury data set is available in digital format through the NEHRI DesignSafe Data Depot at https://doi.org/10.17603/ds2-tygh-ht91. Alternatively, the subsurface data and aerial photographs

are publically available through the New Zealand Geotechnical Database (NZGD 2020) website.

Acknowledgments

This research was funded by National Science Foundation (NSF) Grant Nos. CMMI-1751216, CMMI-1825189, and CMMI-1937984, as well as Pacific Earthquake Engineering Research Center (PEER) Grant No. 1132-NCTRBM and US Geological Survey award G18AP-00006. This support is gratefully acknowledged, as well as access to the NZGD. However, any opinions, findings, and conclusions or recommendations expressed in this paper are those of the authors and do not necessarily reflect the views of NSF, PEER, USGS, or the NZGD.

Supplemental Materials

Fig. S1 and Table S1 are available online in the ASCE Library (www.ascelibrary.org).

References

- Baise, L. G., R. B. Higgins, and C. M. Brankman. 2006. "Liquefaction hazard mapping-statistical and spatial characterization of susceptible units." *J. Geotech. Geoenviron. Eng.* 132 (6): 705–715. https://doi .org/10.1061/(ASCE)1090-0241(2006)132:6(705).
- Beyzaei, C. Z., J. D. Bray, S. van Ballegooy, M. Cubrinovski, and S. Bastin. 2018. "Depositional environment effects on observed liquefaction performance in silt swamps during the Canterbury earthquake sequence." Soil Dyn. Earthquake Eng. 107 (Apr): 303–321. https://doi.org/10.1016 /j.soildyn.2018.01.035.
- Boulanger, R. W., and I. M. Idriss. 2014. CPT and SPT based liquefaction triggering procedures. Rep. No. UCD/CGM-14/01. Davis, CA: Univ. of California at Davis, Dept. of Civil and Environmental Engineering.
- Boulanger, R. W., and I. M. Idriss. 2016. "CPT-based liquefaction triggering procedure." J. Geotech. Geoenviron. Eng. 142 (2): 04015065. https://doi.org/10.1061/(ASCE)GT.1943-5606.0001388.
- Bradley, B. A. 2013a. "A New Zealand-specific pseudo-spectral acceleration ground-motion prediction equation for active shallow crustal earth-quakes based on foreign models." *Bull. Seismol. Soc. Am.* 103 (3): 1801–1822. https://doi.org/10.1785/0120120021.
- Bradley, B. A. 2013b. "Site-specific and spatially-distributed ground motion intensity estimation in the 2010-2011 Christchurch earthquakes." Soil Dyn. Earthquake Eng. 48 (May): 35–47. https://doi.org/10.1016/j.soildyn.2013.01.027.
- Cetin, K. O., R. B. Seed, R. E. Kayen, R. E. S. Moss, H. T. Bilge, M. Ilage, and K. Chowdhury. 2018. "SPT-based probabilistic and deterministic assessment of seismic soil liquefaction triggering hazard." Soil Dyn. Earthquake Eng. 115 (Dec): 698–709. https://doi.org/10.1016/j.soildyn.2018.09.012.
- Chung, J.-W., and J. D. Rogers. 2011. "Simplified method for spatial evaluation of liquefaction potential in the St. Louis area." *J. Geotech. Geoenviron. Eng.* 137 (5): 505–515. https://doi.org/10.1061/(ASCE)GT .1943-5606.0000450.
- Cramer, C. H., G. J. Rix, and K. Tucker. 2008. "Probabilistic liquefaction hazard maps for Memphis, Tennessee." *Seismol. Res. Lett.* 79 (3): 416–423. https://doi.org/10.1785/gssrl.79.3.416.
- Cubrinovski, M., A. Rhodes, N. Ntritsos, and S. Van Ballegooy. 2019. "System response of liquefiable deposits." Soil Dyn. Earthquake Eng. 124 (Sep): 212–229. https://doi.org/10.1016/j.soildyn.2018.05 .013.
- Dixit, J., D. M. Dewaikar, and R. S. Jangid. 2012. "Assessment of lique-faction potential index for Mumbai City." *Nat. Hazards Earth Syst. Sci.* 12 (9): 2759–2768. https://doi.org/10.5194/nhess-12-2759-2012.

- Dobry, R. 1989. "Some basic aspects of soil liquefaction during earth-quakes." Ann. N.Y. Acad. Sci. 558 (1): 172–182. https://doi.org/10.1111/j.1749-6632.1989.tb22567.x.
- Fawcett, T. 2005. "An introduction to ROC analysis." *Pattern Recognit. Lett.* 27 (8): 861–874. https://doi.org/10.1016/j.patrec.2005.10.010.
- Geyin, M., B. W. Maurer, B. A. Bradley, R. A. Green, and S. van Ballegooy. 2021. "CPT-based liquefaction case histories compiled from three earthquakes in Canterbury, New Zealand." *Earthquake Spec*tra37 (4): 2920–2945. https://doi.org/10.1177/8755293021996367.
- Goda, K., and H. P. Hong. 2008. "Spatial correlation of peak ground motions and response spectra." *Bull. Seismol. Soc. Am.* 98 (1): 354–365. https://doi.org/10.1785/0120070078.
- Green, R. A., J. J. Bommer, A. Rodriguez-Marek, B. Maurer, P. Stafford, B. Edwards, P. P. Kruiver, G. de Lange, and J. van Elk. 2019. "Addressing limitations in existing 'simplified' liquefaction triggering evaluation procedures: Application to induced seismicity in the Groningen gas field." Bull. Earthquake Eng. 17 (8): 4539–4557. https://doi.org/10.1007/s10518-018-0489-3.
- Green, R. A., M. Cubrinovski, B. Cox, C. Wood, L. Wotherspoon, B. Bradley, and B. W. Maurer. 2014. "Select liquefaction case histories from the 2010-2011 Canterbury earthquake sequence." *Earthquake Spectra* 30 (1): 131–153. https://doi.org/10.1193/030713EQS066M.
- Green, R. A., B. W. Maurer, and S. van Ballegooy. 2018. "The influence of the non-liquefied crust on the severity of surficial liquefaction manifestations: Case history from the 2016 Valentine's Day earthquake in New Zealand." In Proc., Geotechnical Earthquake Engineering and Soil Dynamics V (GEESD V), Liquefaction Triggering, Consequences, and Mitigation, edited by S. J. Brandenberg and M. T. Manzari, 21–32. Reston, VA: ASCE.
- Green, R. A., S. Upadhyaya, C. M. Wood, B. W. Maurer, B. R. Cox, L. Wotherspoon, B. A. Bradley, and M. Cubrinovski. 2017. "Relative efficacy of CPT- versus Vs-based simplified liquefaction evaluation procedures." In *Proc.*, 19th Intern. Conf. on Soil Mechanics and Geotechnical Engineering. London: International Society of Soil Mechanics and Foundation Engineering.
- Green, R. A., C. Wood, B. Cox, M. Cubrinovski, L. Wotherspoon, B. Bradley, T. Algie, J. Allen, A. Bradshaw, and G. Rix. 2011. "Use of DCP and SASW tests to evaluate liquefaction potential: Predictions vs. observations during the recent New Zealand earthquakes." Seismol. Res. Lett. 82 (6): 927–938. https://doi.org/10.1785/gssrl.82.6.927.
- Hayati, H., and R. D. Andrus. 2008. "Liquefaction potential map of Charleston, South Carolina based on the 1986 earthquake." J. Geotech. Geoenviron. Eng. 134 (6): 815–828. https://doi.org/10.1061/(ASCE) 1090-0241(2008)134:6(815).
- Holzer, T. L. 2008. "Probabilistic liquefaction hazard mapping." Geotechnical earthquake engineering and soil dynamics IV: ASCE geotechnical special publication 181, edited by D. Zeng, M. T. Manzari, and D. R. Hiltunen
- Holzer, T. L., M. J. Bennett, T. E. Noce, A. C. Padovani, and J. C. Tinsley III. 2006. "Liquefaction hazard mapping with LPI in the greater Oakland, California, area." *Earthquake Spectra* 22 (3): 693–708. https://doi.org/10.1193/1.2218591.
- Holzer, T. L., T. E. Noce, and M. J. Bennett. 2009. "Scenario liquefaction hazard maps of Santa Clara Valley, northern California." *Bull. Seismol. Soc. Am.* 99 (1): 367–381. https://doi.org/10.1785/0120080227.
- Ishihara, K. 1985. "Stability of natural deposits during earthquakes." In Proc., 11th Int. Conf. on Soil Mechanics and Foundation Engineering, 376–321. London: International Society of Soil Mechanics and Foundation Engineering.
- Ishihara, K., and K. Ogawa. 1978. "Liquefaction susceptibility map of downtown Tokyo." In *Proc.*, 2nd Int. Conf. on Microzonation, 897–910. Washington, DC: National Science Foundation.
- Ishihara, K., and M. Yoshimine. 1992. "Evaluation of settlements in sand deposits following liquefaction during earthquakes." *Soils Found*. 32 (1): 173–188. https://doi.org/10.3208/sandf1972.32.173.
- Iwasaki, T., F. Tatsuoka, K. Tokida, and S. Yasuda. 1978. "A practical method for assessing soil liquefaction potential based on case studies at various sites in Japan." In *Proc.*, 2nd Int. Conf. on Microzonation, 885–896. Washington, DC: National Science Foundation.

- Kovacs, W. D., and L. A. Salomone. 1984. Field evaluation of SPT energy, equipment, and methods in Japan compared with the SPT in the United States. NBSIR 84-2910. Gaithersburg, MD: National Bureau of Standards.
- Maurer, B. W., R. A. Green, M. Cubrinovski, and B. Bradley. 2015a. "Assessment of CPT-based methods for liquefaction evaluation in a liquefaction potential index framework." *Géotechnique* 65 (5): 328–336. https://doi.org/10.1680/geot.SIP.15.P.007.
- Maurer, B. W., R. A. Green, M. Cubrinovski, and B. Bradley. 2015b. "Calibrating the Liquefaction Severity Number (LSN) for varying misprediction economies: A case study in Christchurch, New Zealand." In *Proc.*, 6th Int. Conf. on Earthquake Geotechnical Engineering. Washington, DC: National Science Foundation.
- Maurer, B. W., R. A. Green, M. Cubrinovski, and B. Bradley. 2015c. "Fines-content effects on liquefaction hazard evaluation for infrastructure during the 2010-2011 Canterbury, New Zealand earthquake sequence." Soil Dyn. Earthquake Eng. 76 (Sep): 58–68. https://doi.org/10.1016/j.soildyn.2014.10.028.
- Maurer, B. W., R. A. Green, M. Cubrinovski, and B. A. Bradley. 2014. "Evaluation of the liquefaction potential index for assessing liquefaction hazard in Christchurch, New Zealand." *J. Geotech. Geoenviron. Eng.* 140 (7): 04014032. https://doi.org/10.1061/(ASCE)GT.1943-5606.0001117.
- Maurer, B. W., R. A. Green, and O. S. Taylor. 2015d. "Moving towards an improved index for assessing liquefaction hazard: Lessons from historical data." Soils Found. 55 (4): 778–787. https://doi.org/10.1016/j.sandf .2015.06.010.
- Maurer, B. W., R. A. Green, S. van Ballegooy, B. A. Bradley, and S. Upadhyaya. 2017a. "Performance comparison of probabilistic and deterministic liquefaction triggering models for hazard assessment in 23 global earthquakes." Geo-Risk 2017: Reliability-Based Design and Code Developments, edited by J. Huang, G. A. Fenton, L. Zhang, and D. V. Griffiths, 31–42. Reston, VA: ASCE.
- Maurer, B. W., R. A. Green, S. van Ballegooy, and L. Wotherspoon. 2017b. "Assessing liquefaction susceptibility using the CPT soil behavior type index." In *Proc.*, *3rd Int. Conf. on Performance-Based Design in Earth-quake Geotechnical Engineering (PBDIII)*. London: International Society of Soil Mechanics and Foundation Engineering.
- Maurer, B. W., R. A. Green, S. van Ballegooy, and L. Wotherspoon. 2019.
 "Development of region-specific soil behavior type index correlations for evaluating liquefaction hazard in Christchurch, New Zealand." Soil Dyn. Earthquake Eng. 117 (Feb): 96–105. https://doi.org/10.1016/j.soildyn.2018.04.059.
- NZGD (New Zealand Geotechnical Database). 2020. "New Zealand geotechnical database." Accessed January 1, 2020. https://www.nzgd.org.nz/.
- Oommen, T., L. G. Baise, and R. Vogel. 2010. "Validation and application of empirical liquefaction models." J. Geotech. Geoenviron. Eng. 136 (12): 1618–1633. https://doi.org/10.1061/(ASCE)GT.1943-5606 .0000395.
- Papathanassiou, G. 2008. "LPI-based approach for calibrating the severity of liquefaction-induced failures and for assessing the probability of liquefaction surface evidence." *Eng. Geol.* 96 (1–2): 94–104. https://doi.org/10.1016/j.enggeo.2007.10.005.
- Papathanassiou, G., S. Pavlides, and A. Ganas. 2005. "The 2003 Lefkada earthquake: Field observation and preliminary microzonation map based on liquefaction potential index for the town of Lefkada." *Eng. Geol.* 82 (1): 12–31. https://doi.org/10.1016/j.enggeo.2005.08.006.
- Robertson, P. K., and C. E. Wride. 1998. "Evaluating cyclic liquefaction potential using cone penetration test." *Can. Geotech. J.* 35 (3): 442–459. https://doi.org/10.1139/t98-017.
- Sana, H., and S. K. Nath. 2016. "Liquefaction potential analysis of the Kashmire Valley alluvium, NW Himalaya." Soil Dyn. Earthquake Eng. 85 (Jun): 11–18. https://doi.org/10.1016/j.soildyn.2016.03.009.
- Sönmez, H. 2003. "Modification of the liquefaction potential index and liquefaction severity mapping for a liquefaction-prone area (Inegol, Turkey)." Eng. Geol. 44 (7): 862–871.
- Tonkin and Taylor. 2013. "Liquefaction vulnerability study." Accessed October 22, 2020. https://www.eqc.govt.nz/sites/public_files/documents/liquefaction-vulnerability-study-final.pdf.

- Ulmer, K. J., R. A. Green, and A. Rodriguez-Marek. 2020. "A consistent correlation between Vs, SPT, and CPT metrics for use in liquefaction evaluation procedures." *Geo-Congress* 2020: *Geotechnical Earthquake Engineering and Special Topics*, edited by J. P. Hambleton, R. Makhnenko, and A. S. Budge, 132–140. Reston, VA: ASCE.
- Upadhyaya, S. 2019. "Development of an improved and internallyconsistent framework for evaluating liquefaction damage potential." Doctoral dissertation, Dept. of Civil and Environmental Engineering, Virginia Tech.
- Upadhyaya, S., R. A. Green, A. Rodriguez-Marek, B. W. Maurer, L. Wotherspoon, B. A. Bradley, and M. Cubrinovski. 2019. "Influence of corrections to recorded peak ground accelerations due to liquefaction on predicted liquefaction response during the M_w 6.2, February 2011 Christchurch earthquake." In *Proc.*, 13th Australia New Zealand Conf. on Geomechanics 2019. St. Ives, Australia: Australian Geomechanics Society.
- Upadhyaya, S., B. W. Maurer, R. A. Green, and A. Rodriguez-Marek. 2018. "Effect of non-liquefiable high fines-content, high plasticity soils on liquefaction potential index (LPI) performance." In *Geotechnical* earthquake engineering and soil dynamics V: Liquefaction triggering, consequences, and mitigation, edited by S. J. Brandenberg and M. T. Manzari, 191–198. Reston, VA: ASCE.
- Upadhyaya, S., B. W. Maurer, R. A. Green, and A. Rodriguez-Marek. 2021. "Selecting optimal factor of safety and probability of liquefaction triggering thresholds for engineering projects based on misprediction costs." J. Geotech. Geoenviron. Eng. 147 (6): 04021026. https://doi .org/10.1061/(ASCE)GT.1943-5606.0002511.
- van Ballegooy, S., S. C. Cox, C. Thurlow, H. K. Rutter, T. Reynolds, G. Harrington, J. Fraser, and T. Smith. 2014a. *Median water table elevation in Christchurch and surrounding area after the 4 September 2010 Darfield earthquake: Version 2*. GNS Science Rep. No. 2014/18. Lower Hutt, New Zealand: GNS Science.
- van Ballegooy, S., R. A. Green, J. Lees, F. Wentz, and B. W. Maurer. 2015. "Assessment of various CPT based liquefaction severity index frameworks relative to the Ishihara (1985) H1-H2 boundary curves." *Soil Dyn. Earthquake Eng.* 79 (Part B): 347–364. https://doi.org/10.1016/j.soildyn.2015.08.015.

- van Ballegooy, S., P. Malan, V. Lacrosse, M. E. Jacka, M. Cubrinovski, J. D. Bray, T. D. O'Rourke, S. A. Crawford, and H. Cowan. 2014b. "Assessment of liquefaction-induced land damage for residential Christ-church." *Earthquake Spectra* 30 (1): 31–55. https://doi.org/10.1193/031813EOS070M.
- van Ballegooy, S., P. J. Malan, M. E. Jacka, V. I. M. F. Lacrosse, J. R. Leeves, J. E. Lyth, and H. Cowan. 2012. "Methods for characterising effects of liquefaction in terms of damage severity." In *Proc., 15th World Conf. on Earthquake Engineering (15 WCEE)*. Tokyo: International Association of Earthquake Engineering.
- Wotherspoon, L. M., R. P. Orense, B. A. Bradley, B. R. Cox, C. Wood, and R. A. Green. 2014. Geotechnical characterisation of Christchurch strong motion stations. Earthquake Commission Biennial Grant Rep. No. 2014, Project No. 12/629. Wellington, New Zealand: New Zealand Earthquake Commission.
- Wotherspoon, L. M., R. P. Orense, R. A. Green, B. A. Bradley, B. R. Cox, and C. M. Wood. 2015. "Assessment of liquefaction evaluation procedures and severity index frameworks at Christchurch strong motion stations." Soil Dyn. Earthquake Eng. 79 (Part B): 335–346. https://doi.org/10.1016/j.soildyn.2015.03.022.
- Yalcin, A., C. Gokceoglu, and H. Sönmez. 2008. "Liquefaction severity map for Aksaray city center (central Anatolia, Turkey)." Natural Hazards Earth Syst. Sci. 8 (4): 641–649. https://doi.org/10.5194/nhess-8 -641-2008.
- Youd, T. L., and C. T. Garris. 1995. "Liquefaction-induced ground surface disruption." J. Geotech. Eng. 121 (11): 805–809.
- Zhang, G., P. K. Robertson, and R. W. I. Brachman. 2002. "Estimating liquefaction-induced ground settlements from CPT for level ground." Can. Geotech. J. 39 (5): 1168–1180. https://doi.org/10.1139/t02-047.
- Zhu, J., L. G. Baise, and E. M. Thompson. 2017. "An updated geospatial liquefaction model for global application." *Bull. Seismol. Soc. Am.* 107 (3): 1365–1385. https://doi.org/10.1785/0120160198.
- Zou, K. H. 2007. "Receiver operating characteristic (ROC) literature research." Accessed March 10, 2016. http://www.spl.harvard.edu/archive/spl-pre2007/pages/ppl/zou/roc.html.